J. Fluid Mech. (2014), *vol.* 756, *pp.* 544–554.
doi:10.1017/jfm.2014.471

Impact dynamics for a floating elastic membrane

L. Duchemin[1,†] **and N. Vandenberghe**[1]

[1]Aix Marseille Université, CNRS, Centrale Marseille, IRPHE UMR 7342, 13384, Marseille, France

(Received 20 May 2014; revised 27 June 2014; accepted 8 August 2014)

We study impacts of a rigid body on a thin elastic sheet floating on a liquid. When struck by a solid object of small size, the elastic sheet deforms and waves propagate in and on the membrane. The impact triggers a longitudinal elastic wave effectively stretching the membrane. The hydroelastic transverse wave that propagates in the stretched domain is similar to capillary waves on a free surface with an equivalent 'surface tension' that results from the stretching of the elastic membrane. Two limiting cases, for which a self-similar solution can be computed, corresponding to short and long times are identified. Surprisingly, our study reveals that the fluid–body system behaves as a regular liquid–gas interface, but with an effective surface tension coefficient that scales linearly with the impact velocity.

Key words: capillary waves, elastic waves, wave–structure interactions

1. Introduction

When transversely impacted by a rigid object, a liquid surface deforms (Korobkin & Pukhnachov 1988). Gravity and/or capillary waves propagate away from the impact point. When a thin elastic body is located at the interface, the wave dynamics is modified. For a body amenable to a two-dimensional description, two different models are considered. Plates, on the one hand, are characterized by a bending rigidity that results in the dynamic boundary condition in a term proportional to $Eh^3\nabla^2\kappa$, where E is Young's modulus of the material (the Poisson ratio is neglected), h the thickness of the elastic sheet and κ its curvature. This elastic response is relevant for moderately thick structures such as ice sheets (Squire *et al.* 1996; Parau & Dias 2002; Milewski, Vanden-Broeck & Wang 2011).

Membranes, on the other hand, are the two-dimensional counterpart of strings: transverse waves can propagate only if the structure is stretched. In the presence of a uniform background in-plane stress σ_b, similar to the tension of a string, the restoring force (per unit surface) in the transverse direction reads $\sigma_b h\nabla^2 w$, where w is the transverse displacement (Landau & Lifshitz 1970). This membrane response is thus formally equivalent to capillary forces at least in the limit of linear waves and the wave dynamics can be described in the context of surface tension dominated impacts (Vella & Metcalfe 2007). This limit is sometimes referred to as the 'waterbed' problem (Press 1978; Srinivasan 1989).

However, when the stretching induced by the impact results in stresses comparable with the background stress, the linear response of the membrane is no longer valid,

† Email address for correspondence: duchemin@irphe.univ-mrs.fr

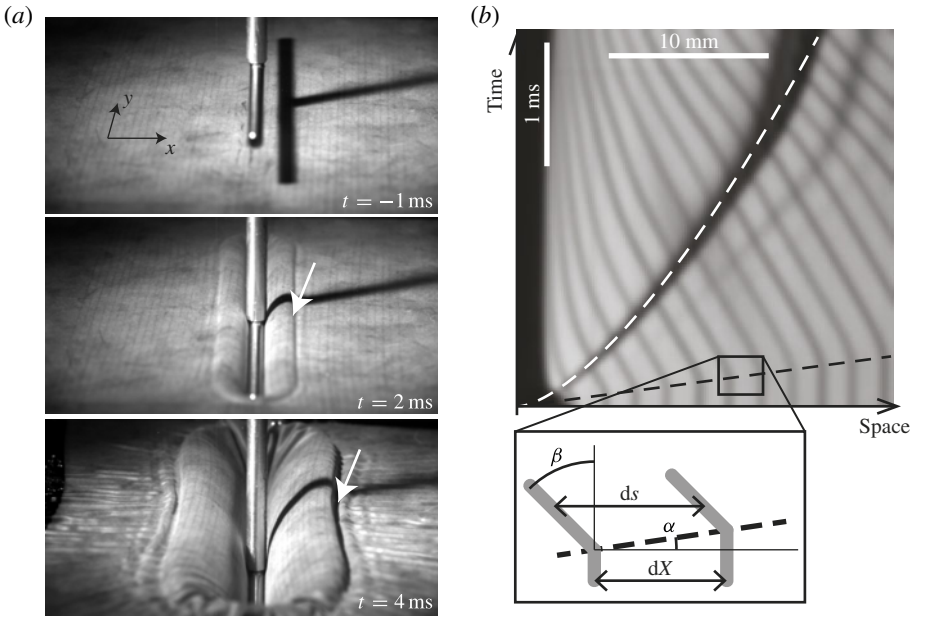

FIGURE 1. (*a*) Floating thin sheet of thickness $h = 0.19$ mm impacted at speed $V = 5.4$ m s^{-1} by a rod of radius 1.75 mm. (*b*) The motion of material points is apparent on a spatiotemporal diagram. The shadow (white arrows on the left) is used as a measure of the position of the transverse wave. The black dashed line shows the longitudinal wave traveling at constant speed ($c = 60$ m s^{-1}) and the white dashed curve $x_f(t) = at^{2/3}$ shows the position of the transverse wavefront (with $a = 9.04$ mm ms$^{-2/3}$). The sketch reveals the strain $\epsilon = \mathrm{d}s/\mathrm{d}X - 1 = \tan\alpha \tan\beta$.

as revealed by experiments in the absence of a liquid substrate (Courbin *et al.* 2006). It is then necessary to describe the coupling between the transverse displacement (along the direction of the impact) and the in-plane displacement (perpendicular to impact direction). In the case of a string or a membrane without background stress, the dynamics results from the coupling between the transverse and longitudinal waves (Phoenix & Porwal 2003; Vermorel, Vandenberghe & Villermaux 2008).

In this study we address the dynamics of the waves that propagate on a floating thin sheet using natural rubber membranes as an experimental system. We neglect the bending rigidity of the membrane, which is initially stress-free. Therefore, the tensile stress, which plays the role of surface tension, is *a priori* unknown and has to be determined.

2. Phenomenology

We perform impact experiments on thin membranes of thickness $h = 0.19$ mm and $h = 0.27$ mm, made of natural rubber (Young's modulus $E = 2.5 \times 10^6$ Pa, Poisson ratio $\nu = 0.5$, density $\rho_m = 920$ kg m^{-3}), floating on water (figure 1). The square membranes, of side length 15 cm, are characterized by their stretching modulus $Y = Eh/(1 - \nu^2)$ and their surface density $\mu = \rho_m h$. They are initially freely floating on water that fills a square tank of side length 40 cm and depth 40 cm. They are not held on their sides, and the background stress caused by surface tension at the air–water-membrane contact line is much smaller than the typical stresses resulting from impact.

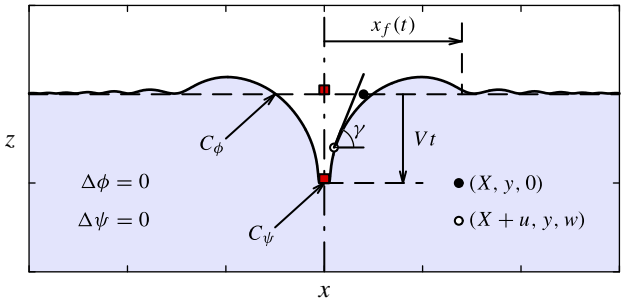

FIGURE 2. (Colour online) Sketch of an impacted floating membrane. Here C_ψ is the part of the membrane underneath the impactor, where the stream function ψ is known at a given time step and the velocity potential ϕ is unknown, and C_ϕ is the part of the membrane (everywhere else) where ϕ is known at a given time step and ψ is unknown.

In the range of strains used in this experiment, the tension in the membrane can be computed through Hooke's law. Nonlinearity of the material, which is significant at higher strains (Albrecht & Ravi-Chandar 2014), are not taken into account.

The impactor is accelerated by a gas gun up to speeds of approximately 10 m s^{-1}. The dynamics is recorded with a high-speed camera. Impacts are performed by a long rod whose axis is in the plane of the floating membrane (xy). The rod (radius 1.75 mm, length 10 cm) together with the guiding axis weighs 29 g, and it does not decelerate during the experiment. It impacts the membranes perpendicularly at their centre.

After impact two different waves propagate in and on the membrane. First a tensile wave, for which material points are moving in the plane of the membrane, is characterized by a well-defined wavefront propagating at constant speed. Behind the tensile wavefront, the membrane is stretched. The strain ϵ can be directly measured from a spatiotemporal diagram (figure 1). The velocity of the material points is uniform and constant. This indicates a constant stretching in the domain delimited by the longitudinal and transverse wavefronts. The transverse wave propagates in the stretched domain, but not at constant speed. In the central region, close to the impactor, a cavity deepens as times goes on. Ahead of the transverse wavefront, ripples of small amplitude travel. At long times, the dynamics changes because the tensile wave interacts with the boundaries of the membrane, and thus the range of timescales that are accessible to experimental investigation is limited.

3. Hydroelastic waves

3.1. *Membrane equations*

In this study, we neglect the displacement along the y direction and discuss the case of a one-dimensional wave. The motion of material points of the membrane is described by the horizontal and vertical components of their displacement $u(X, t)$ and $w(X, t)$, where X is the coordinate of the material point in the reference (undeformed) configuration (figure 2)

$$\mu \,\mathrm{d}X \partial_{tt} u = \partial_X \left(T \cos\gamma\right) \,\mathrm{d}X - p \,\mathrm{d}s \sin\gamma, \tag{3.1}$$

$$\mu \,\mathrm{d}X \partial_{tt} w = \partial_X \left(T \sin\gamma\right) \,\mathrm{d}X + p \,\mathrm{d}s \cos\gamma. \tag{3.2}$$

Here T is the tension in the elastic membrane. It is related to the strain $\epsilon = \mathrm{d}s/\mathrm{d}X - 1 = [(1 + \partial_X u)^2 + (\partial_X w)^2]^{1/2} - 1$ through Hooke's law, $T = Y\epsilon$. We use γ to denote

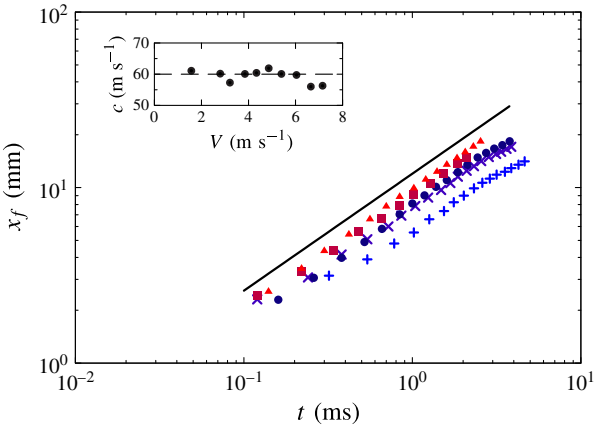

FIGURE 3. (Colour online) Position of the transverse wavefront for a 2D impact on a membrane of thickness $h = 0.19$ mm at impact speeds $V = 1.57$ m s^{-1} (+), 3.21 m s^{-1} (×), 4.34 m s^{-1} (●), 5.40 m s^{-1} (■) and 7.15 m s^{-1} (▲). The solid line shows the scaling law $x_f \sim t^{2/3}$. The longitudinal wave speed c, measured on spatiotemporal diagrams, is constant (inset).

the angle between the membrane and the X-axis and p is the pressure exerted by the lower fluid on the membrane. These two equations can be rewritten

$$\mu \cos\gamma\, \partial_{tt} w - \mu \sin\gamma\, \partial_{tt} u = T \partial_X \gamma + (1+\epsilon) p \tag{3.3}$$

$$\mu \sin\gamma\, \partial_{tt} w + \mu \cos\gamma\, \partial_{tt} u = \partial_X T. \tag{3.4}$$

In the region where $|\tan\gamma| \ll 1$, the strain simplifies to $\epsilon \approx \partial_X u$, and the equation for the longitudinal displacement reduces to a wave equation

$$\partial_{tt} u = c^2 \partial_{XX} u, \tag{3.5}$$

where $c = (Y/\mu)^{1/2}$ is a material property, independent of h and of impact speed (figure 3). Equation (3.5) admits solutions in the form of a step function propagating at speed c as observed in the experiments, at least in the domain with small slopes $\partial_X w$. However, this equation does not give any clue on the amplitude of the stretching.

Assuming that the membrane is in internal equilibrium, at each instant, in the longitudinal direction, between the impactor and the tensile wavefront located in $X = ct$, the inertial terms in (3.4) can be neglected, yielding

$$\epsilon = \epsilon_0 = C^{st}. \tag{3.6}$$

If the inertial terms in (3.3) are neglected, the membrane can be treated as an interface and (3.3) is then equivalent to Laplace's law

$$p = -Y\epsilon_0 \kappa, \tag{3.7}$$

where $\kappa = \partial_s \gamma = \partial_X \gamma/(1+\epsilon_0)$ is the local curvature of the membrane. In the experiment, typical values of the strain lie between 0.01 and 0.1; therefore, the effective surface tension coefficient $Y\epsilon_0$ ranges from 5 to 50 N m^{-1}, which is two

or three orders of magnitude larger than the air/water surface tension coefficient, and corresponds to a capillary length $\sqrt{Y\epsilon_0/\rho g}$ between 2 and 7 cm.

3.2. *Inviscid fluid equations*

We neglect viscous effects in the liquid underneath the membrane and, in particular, the effect of the boundary layer that accompanies the longitudinal motion of the material points (Vermorel, Vandenberghe & Villermaux 2006). The irrotational two-dimensional motion of an ideal fluid of density ρ is described using the velocity potential $\phi(x, z, t)$ (here x, z are spatial coordinates) which satisfies Laplace's equation in the bulk

$$\nabla^2\phi = 0, \tag{3.8}$$

and the kinematic and dynamic boundary conditions at $z = w(x, t)$

$$\partial_t w = \partial_z\phi - \partial_x\phi\partial_x w, \tag{3.9}$$

$$\partial_t\phi + \frac{1}{2}|\nabla\phi|^2 - \frac{Y\epsilon_0}{\rho}\kappa = 0, \tag{3.10}$$

where $\kappa = \partial_{xx}w/(1 + \partial_x w^2)^{3/2}$ is the curvature and (3.7) has been used to express the pressure underneath the membrane. Additional inertial terms proportional to μ are omitted because, for transverse waves with a wavelength longer than h, the inertia associated with the fluid dominates. A gravitational term gw in the left-hand side of (3.10) has been omitted because the length scales in the experiment are shorter than the capillary length.

Equation (3.10), together with the kinematic boundary condition (3.9) and Laplace's equation (3.8), describes a flow driven by surface tension (Keller & Miksis 1983). After impact at $t = 0$, the transverse perturbation of the surface travels in the x direction according to a scaling law of the form $at^{2/3}$ where $a \sim (Y\epsilon_0/\rho)^{1/3}$. This self-similar behaviour can be seen in the transverse wavefront position $x_f(t)$ (figure 2) and is in very good agreement with the experiments, for a large range of impact velocities, as seen in figure 3. Moreover, the prefactor a increases with the impact velocity, as will be discussed in details in § 5.

4. Self-similar solutions

The equations can be made non-dimensional using $L' = Y\epsilon_0/\rho V^2$, L'/V and ρ as the length, time and density scales, respectively. In our experiments, the width of the impactor L is always smaller than L' and the capillary length $\sqrt{Y\epsilon_0/\rho g}$ (Vella & Li 2010). Therefore, we treat the impactor as a point.

4.1. *Short-time dynamics*

The wave equations admit a self-similar solution at short times (i.e. non-dimensional times shorter than 1) (Vella & Metcalfe 2007). The vertical scale is imposed by the z coordinate of the impactor, $-t$ in dimensionless units and the horizontal scale is the transverse wavefront position $t^{2/3}$ in dimensionless units. In the bulk, to balance the two terms in (3.8), the scalings in x and z are the same. The time dependence of the velocity potential is imposed by the balance of dominant terms in (3.8)–(3.10). Therefore, using the ansatz

$$w(x, t) = tW(x/t^{2/3}) \quad \text{and} \quad \phi(x, z, t) = t^{2/3}\Phi(x/t^{2/3}, z/t^{2/3}), \tag{4.1a,b}$$

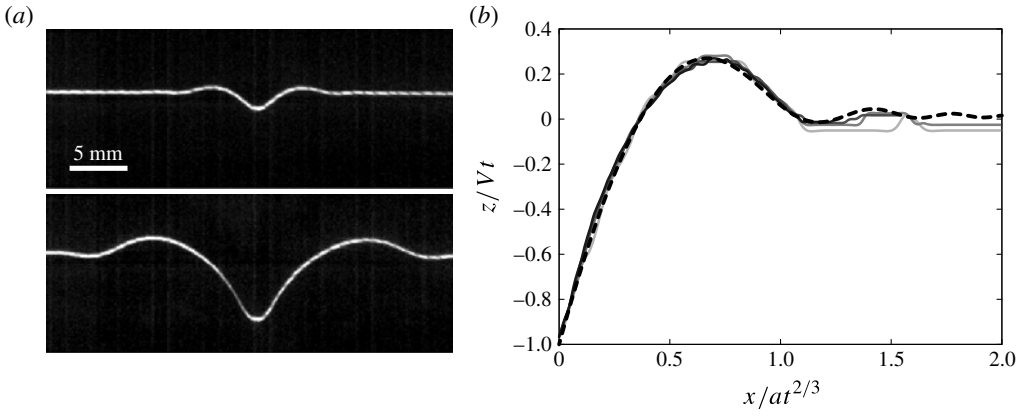

FIGURE 4. (*a*) Successive profiles of the membrane in the short-time range at $V = 1.3$ m s^{-1}, for $t = 1$ and 4 ms. (*b*) Scaled experimental profiles (from light grey for 1 ms to dark grey for 4 ms by steps of 1 ms), and solution to (4.2)–(4.6) (dashed).

one obtains, to leading order in t, the following linear system of equations

$$\eta \leqslant 0 : \nabla^2 \Phi = 0, \tag{4.2}$$

$$\eta = 0 : W(\xi) - \tfrac{2}{3}\xi W'(\xi) = \partial_\eta \Phi(\xi, 0), \tag{4.3}$$

$$\eta = 0 : \tfrac{2}{3}\Phi - \tfrac{2}{3}\xi \partial_\xi \Phi(\xi, 0) - W''(\xi) = 0, \tag{4.4}$$

$$\xi = 0 : W(0) = -1, \tag{4.5}$$

$$\xi = 0 : \partial_\xi \Phi(0, \eta) = 0, \tag{4.6}$$

where $\xi = x/t^{2/3}$ and $\eta = z/t^{2/3}$, and the discarded terms are all of the order of $t^{1/3}$ or smaller. We have solved this system of equations, using centred finite differences for (4.3) and (4.4) and a series expansion of Φ that satisfies (4.2) in the domain $(\xi, \eta) \in ([0, \lambda],]-\infty, 0])$, and the boundary condition (4.6)

$$\Phi = \sum_k \alpha_k \mathrm{e}^{2\pi k \eta/\lambda} \cos(2\pi k \xi/\lambda), \tag{4.7}$$

where λ is a length much larger than the typical scale of variations of the solution. Figure 4 shows a comparison of the experimental profiles at small speed, scaled according to $at^{2/3} = x_f(t)$ and Vt, with the solution to (4.2)–(4.6). The theoretical solution has been scaled on the x direction by a factor 2.5, to match the experimental profiles in $x_f(t)/at^{2/3} = 1$.

Equations (4.2)–(4.6) have been obtained in a small-slope approximation. Indeed, the local slope of the membrane reads $\partial_x w = t^{1/3} W'(\xi)$ and is effectively small as long as $t \ll 1$. Therefore, as time increases, this approximation becomes irrelevant, and the terms in $t^{1/3}$ are no longer negligible. The inset in figure 5 shows that this short-time scaling is not as accurate as the long-time dynamics described below. These data were obtained at higher impact speed, which corresponds to higher aspect ratio $Vt/x_f(t)$ and thus to 'long times' in our experiments.

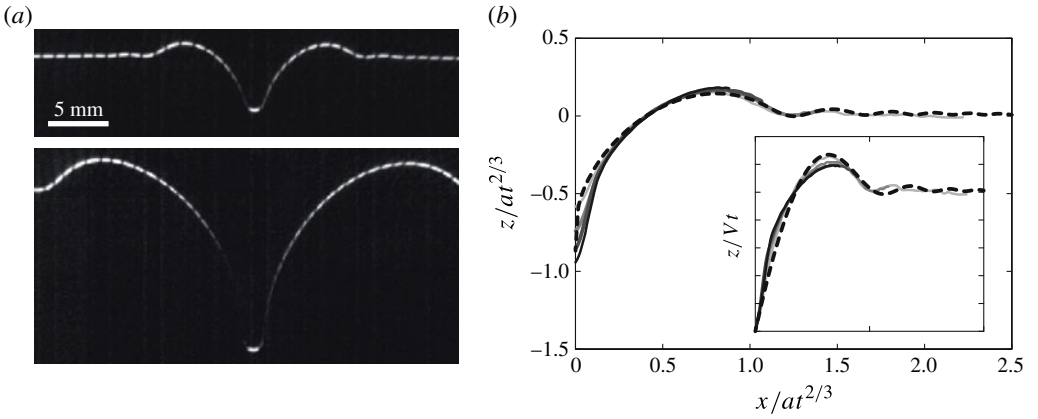

FIGURE 5. (*a*) Successive profiles of the membrane in the long-time range at $V = 4.30$ m s^{-1}, for $t = 1$ and 3 ms. (*b*) Scaled experimental profiles (from light grey for 1 ms to dark grey for 4 ms), and solution to (4.9)–(4.11) (dashed). In the inset, the profiles have been rescaled according to $at^{2/3} = x_f(t)$ along x and Vt along z; the dashed curve in black is the solution to (4.2)–(4.6).

4.2. *Long-time dynamics*

At long times, the experimental results suggest that the membrane dynamics enters another regime for which the length scales in both directions, x and z, are proportional to $t^{2/3}$, as seen in figure 5. Using the variables $\xi = x/t^{2/3}$ and $\eta = z/t^{2/3}$, with the ansatz (Keller & Miksis 1983)

$$w(x, t) = t^{2/3} W(x/t^{2/3}) \quad \text{and} \quad \phi(x, z, t) = t^{1/3} \Phi(x/t^{2/3}, z/t^{2/3}), \tag{4.8a,b}$$

all of the terms are balanced in the equations, and we obtain the following system of nonlinear equations

$$\eta \leqslant W(\xi) : \nabla^2 \Phi = 0, \tag{4.9}$$

$$\eta = W(\xi) : \tfrac{2}{3} W(\xi) - \tfrac{2}{3} \xi W'(\xi) = \partial_\eta \Phi(\xi, \eta) - \partial_\xi \Phi(\xi, \eta) \partial_\xi W(\xi), \tag{4.10}$$

$$\eta = W(\xi) : \tfrac{1}{3} \Phi - \tfrac{2}{3} \xi \partial_\xi \Phi(\xi, \eta) + \tfrac{1}{2} \nabla \Phi^2 - W''(\xi)/(1 + W'(\xi)^2)^{3/2} = 0, \tag{4.11}$$

with the boundary condition at the impactor $W(0) = -Vt^{1/3}$. A self-similar solution to this problem does not exist because of the time-dependent boundary condition. However, for $t \to \infty$, a limit solution can be sought for using the same integrodifferential system of equations as in Keller & Miksis (1983). We solve this system of equations, imposing a horizontal surface as $\xi \to \infty$ and decreasing the angle θ between the z-axis and the membrane in $x = 0$. As θ decreases, the height of the first bump reaches a constant value, while the vertical coordinate $W(0)$ keeps decreasing (right inset of figure 6), suggesting that the solution converges towards a unique shape. This shape is compared, after rescaling by a factor 2.5, with experimental results in figure 5.

The long-time behaviour is also investigated through a numerical computation using a boundary integral method (see the Appendix). Figure 6 shows successive profiles of the numerical solution and a comparison of these numerical profiles rescaled with respect to $t^{2/3}$ with the limit solution to (4.9)–(4.11), described above. The

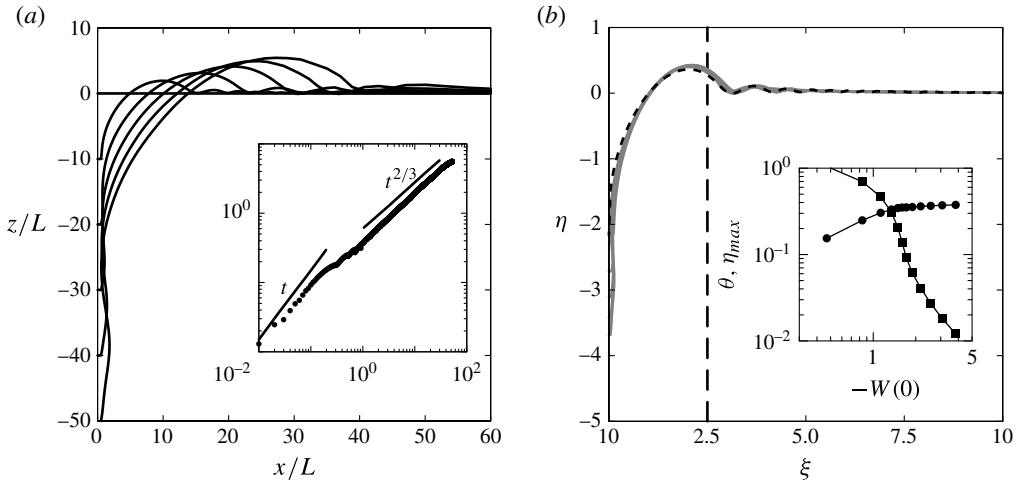

FIGURE 6. Long-time dynamics. (*a*) Successive shapes obtained with a boundary integral method. The size of the impactor L is used as the reference length. Inset: vertical coordinate of the first bump height on the membrane as a function of time, and the short- and long-time behaviours in t and $t^{2/3}$ respectively. (*b*) In grey: collapsed rescaled numerical profiles. Dashed curve: solution to Keller and Miksis system of equations, for an angle θ between the z-axis and the membrane in $x = 0$, equal to 0.04 rad. Inset: for (4.9)–(4.11), when $-W(0)$ increases, the angle θ decreases (■), while the first bump height η_{max} reaches a constant value (●).

rescaled profiles and the theoretical solution are superimposed, except in the region of the impactor as expected, showing that the full dynamics of the impact, in the limit of long times, can be seen as a self-similar surface tension driven flow. The time-dependent boundary condition at the impactor explains, as in Peters, Van Der Meer & Gordillo (2013), why the z scaling of the membrane is not exactly $t^{2/3}$, as seen in the left inset of figure 6.

5. What sets ϵ_0?

So far, we have treated the membrane as a constant surface tension interface. However, the surface tension coefficient $\sigma = Y\epsilon_0$ obtained in (3.6) does depend on the impact speed (figure 3). The value of ϵ_0 can be obtained in two different ways of analysing the experimental results: the strain can be directly measured on spatiotemporal diagrams (figure 1) and ϵ_0 can be inferred from the dynamics of the transverse wavefront. Indeed, coming back to dimensional variables, the horizontal position of the front reads

$$x_f(t) \approx 2.5 \left(\frac{Y\epsilon_0}{\rho}\right)^{1/3} t^{2/3}. \tag{5.1}$$

Then, ϵ_0 can be extracted from the prefactor in the evolution of $x_f(t)$. Both measurements are in quantitative agreement: ϵ_0 is linear in the impact velocity V, as seen in figure 7.

The simplest approach that yields a prediction for ϵ_0 consists in the following idealization. We use the fact that the membrane is very steep around the impactor

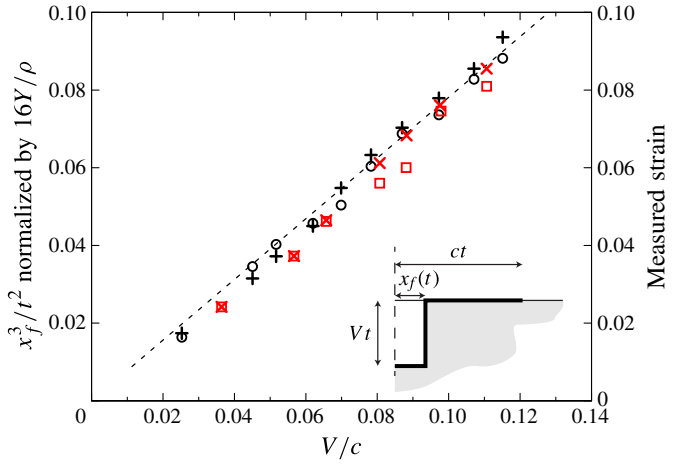

FIGURE 7. (Colour online) Strain measured on the experiments, as a function of V/c. Left axis (○, □): as $(\rho/16Y)x_f^3/t^2$ (note that $2.5^3 \simeq 16$). Right axis (+, ×): directly measured on spatiotemporal diagrams. (○, +) and (□, ×) symbols correspond to membranes of thickness $h = 0.19$ and 0.27 mm, respectively. Inset: sketch of a punched membrane.

at large times and consider that the cavity is a rectangle of height Vt and width $x_f(t) \ll Vt$ (i.e. a punched membrane). Thus, the stretching is given by the relation $\epsilon_0 = (\ell - \ell_0)/\ell_0$ where $\ell_0 = ct$ and ℓ is the length of the broken line that extends from ct to the impact point:

$$\epsilon_0 \approx \frac{(Vt + ct) - ct}{ct} = \frac{V}{c}. \tag{5.2}$$

This approximation is valid for large times, when $Vt > x_f$, but the measurements (figure 1) suggest that the value $\epsilon_0 \approx V/c$ is reached very early in the experiments. We note that in the experiments, $\epsilon_0 \approx 0.78\ V/c$. The prefactor results from the geometry of the cavity, not accounted for in our simplified model.

6. Concluding remarks

The impact dynamics on a floating membrane exhibits two distinct waves, a longitudinal wave that propagates at constant speed and a transverse wave that exhibits the typical self-similar behaviour of surface-tension-driven flows. Two different behaviours are observed, at short and long time scales, the cross-over time being $Y/(\rho c V^2)$. The geometry imposed by the two propagating waves imposes the strain, and the effective surface tension coefficient depends linearly on impact speed. The situation presented here, with two waves and a variable surface tension is similar to the impact on thin surfactant-coated lamellae (Thomas & Davies 1974), for which the variation of surface tension results from variations of surfactant concentration induced by stretching.

A natural extension of this work is the case of an axisymmetric impact. However, the axisymmetric case requires a much more refined treatment of the membrane dynamics because the strain on a membrane experiencing a punctual impact is not uniform. Although we expect similarities with the present case, in particular the two waves dynamics, we leave the axisymmetric case as a perspective of this work.

Acknowledgement

We acknowledge support from the Agence Nationale de la Recherche through grant ANR-11-JS09-0005.

Appendix A. Details of the numerical method

To solve Laplace's equation (3.8) in the fluid domain, with boundary conditions (3.9), (3.10), and an imposed velocity underneath the impactor equal to $-\boldsymbol{e}_z$, we define a complex potential $\beta(\zeta) = \phi + \mathrm{i}\psi$, where $\zeta = x + \mathrm{i}z$, ψ is the stream function and β is related to the horizontal and vertical components of the velocity field through

$$\frac{\mathrm{d}\beta}{\mathrm{d}\zeta} = u - \mathrm{i}v. \tag{A 1}$$

Once β is known everywhere on the membrane and underneath the impactor, the fluid velocity can be computed, and (3.9) and (3.10) can be advanced in time.

For a point ζ_0 on the membrane, β obeys Cauchy's integral theorem

$$\mathrm{i}\pi\beta(\zeta_0) = -\fint_{-\infty}^{+\infty} \frac{\beta(\zeta)}{\zeta - \zeta_0}\,\mathrm{d}\zeta, \tag{A 2}$$

where the integral is a principal value integral.

We divide the membrane into two sets (figure 2): C_ϕ where ϕ is known and ψ is unknown, and the lower impactor's surface C_ψ where ψ is known and ϕ is unknown. When ζ_0 is on C_ϕ, the real part of (A 2) is a Fredholm integral equation of the second kind for ψ, which is known to have a unique solution; when ζ_0 is on C_ψ, the imaginary part of (A 2) is a Fredholm integral equation of the second kind for ϕ. On C_ψ, $\psi = Vx$ to account for the constant vertical velocity of the impactor $v = -V = -\partial_x\psi$.

Assuming that β is linear in ζ between two successive points on the membrane, the logarithmic singularities occurring in the principle value integral can be integrated exactly. Equation (A 2) is therefore written as a system of linear equations for the values of ψ on C_ϕ and ϕ on C_ψ, and solved using an LU decomposition. When $\zeta \to \pm\infty$, the surface is supposed to be flat, and β is approximated by the complex potential due to a dipole placed at the origin: $\beta \sim \alpha/\zeta$.

Once ϕ and ψ are known everywhere on the membrane, the velocity components u and v are computed through (A 1) using second-order centred finite differences along the membrane. Finally, (3.9) and (3.10) are advanced in time, from t to $t + \delta t$, using a second-order explicit time-integration scheme.

When solving with a punctual impactor, we encountered self-intersection of the membrane in the region of the impactor, which prevented us from computing the long-time dynamics. Therefore, we had to do the computation with a finite-size impactor, and used its width L as the reference length. For the value of the Weber number, we chose $We = L/L' = \rho L V^2/Y\epsilon_0 = 1$, which corresponds to high-speed experimental conditions.

REFERENCES

ALBRECHT, A. B. & RAVI-CHANDAR, K. 2014 High strain rate response of rubber membranes. *J. Mech. Phys. Solids* **64**, 377–395.

COURBIN, L., MARCHAND, A., VAZIRI, A., AJDARI, A. & STONE, H. A. 2006 Impact dynamics for elastic membranes. *Phys. Rev. Lett.* **97**, 244301.

KELLER, J. B. & MIKSIS, M. J. 1983 Surface tension driven flows. *SIAM J. Appl. Maths* **43** (2), 268–277.

KOROBKIN, A. A. & PUKHNACHOV, V. V. 1988 Initial stage of water impact. *Annu. Rev. Fluid Mech.* **20**, 159–185.

LANDAU, L. D. & LIFSHITZ, E. M. 1970 *Theory of Elasticity*. Pergamon Press.

MILEWSKI, P. A., VANDEN-BROECK, J. M. & WANG, Z. 2011 Hydroelastic solitary waves in deep water. *J. Fluid Mech.* **679** (1), 628–640.

PARAU, E. & DIAS, F. 2002 Nonlinear effects in the response of a floating ice plate to a moving load. *J. Fluid Mech.* **460**, 281–305.

PETERS, I. R., VAN DER MEER, D. & GORDILLO, J. M. 2013 Splash wave and crown breakup after disc impact on a liquid surface. *J. Fluid Mech.* **724**, 553–580.

PHOENIX, S. L. & PORWAL, P. K. 2003 A new membrane model for the ballistic impact response and V50 performance of multi-ply fibrous systems. *Intl J. Solids Struct.* **40** (24), 6723–6765.

PRESS, W. H. 1978 Mathematical theory of the waterbed. *Am. J. Phys.* **46** (10), 966–970.

SQUIRE, V., HOSKING, R. J., KERR, A. D. & LANGHORNE, P. J. 1996 *Moving Loads on Ice Plates*. Kluwer.

SRINIVASAN, M. A. 1989 Surface deflection of primate fingertip under line load. *J. Biomech.* **22** (4), 343–349.

THOMAS, T. B. & DAVIES, J. T. 1974 On the sudden stretching of liquid lamellae. *J. Colloid Interface Sci.* **48** (3), 427–436.

VELLA, D. & LI, J. 2010 The impulsive motion of a small cylinder at an interface. *Phys. Fluids* **22** (5), 052104.

VELLA, D. & METCALFE, P. D. 2007 Surface tension dominated impact. *Phys. Fluids* **19** (7), 072108.

VERMOREL, R., VANDENBERGHE, N. & VILLERMAUX, E. 2006 Rubber band recoil. *Proc. R. Soc. Lond.* A **463** (2079), 641–658.

VERMOREL, R., VANDENBERGHE, N. & VILLERMAUX, E. 2008 Impacts on thin elastic sheets. *Proc. R. Soc. Lond.* A **465** (2103), 823–842.